Progress In Electromagnetics Research, Vol. 128, 399–418, 2012

SPECIFIC ABSORPTION RATE COMPUTATIONS WITH A NODAL-BASED FINITE ELEMENT FORMULATION

R. Otin[1, *] and H. Gromat[2]

[1]CIMNE — International Center for Numerical Methods in Engineering, Parque Mediterráneo de la Tecnología (PMT), c/ Esteve Terradas 5-Edificio C3-Despacho 206, 08860 Castelldefels, Barcelona, Spain

[2]CASSIDIAN, MetaPole ZAC La Clef Saint-Pierre, 1, Boulevard Jean Moulin-CS 40001, 78996 Elancourt Cedex, France

Abstract—The aim of this work is to asses the performance of a nodal-based finite element formulation when applied to the computation of specific absorption rate (SAR) problems. This formulation solves numerically the regularized Maxwell equations using nodal elements and, in principle, it offers several advantages: It provides spurious-free solutions and well-conditioned matrices without the need of Lagrange multipliers or scalar potentials. Its integral representation is well-suited for hybridization with integral numerical techniques because of a low-order singular kernel. Also, the nodal approximation of the electromagnetic problem is easier to couple to a thermal finite element problem which usually also employs nodal elements. But, on the other hand, we need to take special care of the points of the domain where the field is singular to obtain accurate solutions. In this paper, we show the impact of the singularities on the performance of the proposed finite element formulation and how its good features are affected when solving real-life SAR problems.

1. INTRODUCTION

The specific absorption rate (SAR) is the power per unit mass absorbed by a body when illuminated by electromagnetic fields. This quantity is useful to determine, in combination with the heat equation, the temperature increase produced by the incident electromagnetic radiation inside the body, as done in [22]. The SAR is helpful to determine the levels of radiation which are below dangerous limits and

Received 11 April 2012, Accepted 14 May 2012, Scheduled 2 June 2012

* Corresponding author: Ruben Otin (rotin@cimne.upc.edu).

can be safely used in therapeutic treatments [23, 25, 27]. The SAR is also a quantity used for regulatory purposes. That is, before a mobile phone is available for sale to the general public, it must shown that the SAR is below some limits. In addition, a mobile phone with a high value of SAR implies that the energy of the battery is wasted in unwanted heating instead of being used to transmit information [21].

The measurement of the SAR is performed in specialized test houses with complex and sophisticated systems. Besides, if you want your product to comply with government requirements, you have to send it to an accredited test house to obtain the certification. This process is expensive and time-consuming. Numerical simulations can save time and money predicting the value of the SAR before certification and improving the design of the product before manufacturing it. Also, numerical simulations are of valuable help when we need to know the SAR in places where its measurement is difficult, like inside the bodies of living creatures [23, 26, 28].

In the scenario present above, the regularized nodal-based finite element formulation proposed in this work seems to be a good choice for the computation of the SAR. This is so because, in principle, this approach presents several advantages:

- The finite element method (FEM) works naturally with complex geometries and materials.
- The FEM numerical approximation of the regularized Maxwell equations provides spurious-free solutions and well-conditioned matrices that are easy to solve with iterative Krylov solvers [1].
- Only the three components of the electric field $\mathbf{E}$ are the unknowns; that is, there is no need of extra functions such as Lagrange multipliers or scalar potentials.
- The integral representation of the regularized Maxwell equations involves a singular kernel of order 1 instead of the order 3 found in the double-curl formulation with edge elements [1]. This fact makes the regularized FEM formulation best suited to hybridization with integral numerical techniques [20].
- The nodal FEM solution of the electromagnetic problem is easier to couple to thermo-mechanical multi-physics problems which usually also employ nodal FEM elements [22].

But, on the other hand, we need a special treatment on the points of the problem domain where the field is singular and/or discontinuous. In [2] it is explained the techniques we need to apply on these points to obtain accurate solutions. In this paper, we show the effect of these corrections on the regularized formulation when solving real-life SAR problems.

2. DEFINITIONS

The specific absorption rate (SAR) is defined as,

$$\mathrm{SAR}\,(\mathrm{W/kg}) = \frac{\sigma + \omega\epsilon''}{2\rho}\,|\mathbf{E}|^2 \tag{1}$$

where σ is the electrical conductivity, ρ is the mass density, ω is the angular frequency, ϵ'' is the imaginary part of the electric permittivity $\varepsilon = \epsilon' + i(\epsilon'' + \sigma/\omega)$ and $\mathbf{E}$ is the electric field. The expression (1) represents the time-average power per unit mass dissipated as heat due to conductivity and dielectric losses. This expression is deduced from the Poynting's theorem assuming time-harmonic fields, linear materials and no magnetic losses. In this work, we will compute numerically the field $\mathbf{E}$ to obtain the SAR.

When the SAR is employed for regulatory purposes it is usually averaged either over the whole body, or over a small sample volume (typically 1 g or 10 g of tissue). SAR limits for a radiating object depends on the country, for instance, in United States, the Federal Communications Commission (FCC) requires that phones sold for the general public have a SAR level at or below 1.6 W/kg taken over a volume of 1 g of tissue with the shape of a cube. In the European Union, before a mobile phone is available for sale, it must show compliance with the European Radio & Telecommunication Terminal Equipment (R & TTE) directive 1999/5/EC. This directive limits the human exposure to radio frequency (RF) fields in accordance with the standard EN 50360 : 2001 developed by the European Committee for Electrotechnical Standardization (CENELEC). This standard is summarized in Table 1.

3. FINITE ELEMENT FORMULATION

In this work, the electric field $\mathbf{E}$ appearing in (1) is computed by solving numerically the regularized time-harmonic Maxwell's wave

Table 1. SAR limits specified by the CENELEC EN 50360 : 2001. $\mathrm{SAR_{wb}}$ is the average over the whole body. $\mathrm{SAR_{10g}}$ is the average over 10 g of tissue with the shape of a cube.

Type of user	$\mathrm{SAR_{wb}}$ (W/Kg)	$\mathrm{SAR_{10g}}$ (W/Kg)
General public	0.08	2
Occupational	0.40	10

Equation [1]

$$\nabla \times \left(\frac{1}{\mu} \nabla \times \mathbf{E} \right) - \bar{\varepsilon} \nabla \left(\frac{1}{\bar{\varepsilon} \varepsilon \mu} \nabla \cdot (\varepsilon \mathbf{E}) \right) - \omega^2 \varepsilon \mathbf{E} = i\omega \mathbf{J}, \tag{2}$$

where μ is the magnetic permeability, ε is the electric permittivity, $i = \sqrt{-1}$ is the imaginary unit and $\mathbf{J}$ is an imposed current density. The bar over a magnitude denotes its complex conjugate. If we solve Equation (2) in an open domain Ω, we must apply a regularized version of the Silver-M*ü*ller radiation boundary condition at infinity [1]

$$\lim_{r \to \infty} \oint_{\partial \Omega_r} \left\| \hat{\mathbf{n}} \times \nabla \times \mathbf{E} - ik_0 \left(\hat{\mathbf{n}} \times \hat{\mathbf{n}} \times \mathbf{E} \right) \right\|^2 = 0,$$

$$\lim_{r \to \infty} \oint_{\partial \Omega_r} \left| \nabla \cdot \mathbf{E} - ik_0 \left(\hat{\mathbf{n}} \cdot \mathbf{E} \right) \right|^2 = 0. \tag{3}$$

where $\partial \Omega_r$ is the boundary of the domain Ω at a distance r from the sources and $k_0 = \omega \sqrt{\epsilon_0 \mu_0}$, being ϵ_0 and μ_0, respectively, the electric permittivity and the magnetic permeability of vacuum. On the surface of a perfect electric conductor (PEC) we impose the regularized version of the standard PEC boundary condition [1]

$$\begin{aligned} \nabla \cdot (\varepsilon \mathbf{E}) &= 0, \\ \hat{\mathbf{n}} \times \mathbf{E} &= 0, \end{aligned} \tag{4}$$

where $\hat{\mathbf{n}}$ is the exterior unit normal of the PEC surface.

The second-order differential Equation (2) with boundary conditions (3) and (4) can also be solved using an equivalent weak formulation. That is, if we define

$$\mathbf{H}\left(\mathbf{curl}, \mathrm{div}; \Omega\right) := \left\{ \mathbf{F} \in \mathbf{L}^2\left(\Omega\right) \middle| \nabla \times \mathbf{F} \in \mathbf{L}^2\left(\Omega\right), \nabla \cdot (\varepsilon \mathbf{F}) \in L^2\left(\Omega\right) \right\}, \tag{5}$$

being $L^2\left(\Omega\right)$ the space of square integrable functions in the domain Ω and $\mathbf{L}^2\left(\Omega\right)$ the space of vectorial functions with all its components belonging to $L^2\left(\Omega\right)$, and

$$\mathbf{H}_0\left(\mathbf{curl}, \mathrm{div}; \Omega\right) := \{ \mathbf{F} \in \mathbf{H}\left(\mathbf{curl}, \mathrm{div}; \Omega\right) \mid \hat{\mathbf{n}} \times \mathbf{F} = 0 \text{ in PEC} \}. \tag{6}$$

Then, solving the problem represented by Equations (2) to (4) is equivalent to finding $\mathbf{E} \in \mathbf{H}_0(\mathbf{curl}, \mathrm{div}; \Omega)$ such that $\forall \mathbf{F} \in \mathbf{H}_0(\mathbf{curl}, \mathrm{div}; \Omega)$ holds:

$$\begin{aligned} &\int_\Omega \frac{1}{\mu} \left(\nabla \times \mathbf{E}\right) \cdot \left(\nabla \times \bar{\mathbf{F}}\right) + \int_\Omega \frac{1}{\mu \varepsilon \bar{\varepsilon}} \left(\nabla \cdot (\varepsilon \mathbf{E})\right) \cdot \left(\nabla \cdot \left(\bar{\varepsilon} \bar{\mathbf{F}}\right)\right) - \omega^2 \int_\Omega \varepsilon \left(\mathbf{E} \cdot \bar{\mathbf{F}}\right) \\ &- \int_{\partial \Omega} \frac{1}{\mu} \left(\nabla \times \mathbf{E}\right) \cdot \left(\hat{\mathbf{n}} \times \bar{\mathbf{F}}\right) - \int_{\partial \Omega} \frac{1}{\mu \varepsilon \bar{\varepsilon}} \left(\nabla \cdot (\varepsilon \mathbf{E})\right) \cdot \left(\hat{\mathbf{n}} \cdot \left(\bar{\varepsilon} \bar{\mathbf{F}}\right)\right) = i\omega \int_\Omega \mathbf{J} \cdot \bar{\mathbf{F}}, \end{aligned} \tag{7}$$

where $\partial \Omega$ is the boundary of the domain Ω. In [1] it is shown that solving analytically the *regularized* weak formulation (7) is completely

equivalent to solving the *classical* double-curl time-harmonic Maxwell's wave equation. The regularized formulation (7) presents all the advantages detailed at the introduction of this paper when it is solved with nodal (Lagrangian) finite elements. However, we must be careful if the electric field **E** is singular at some point of the domain. In such a case, the physical solution can not be approximated with nodal elements and (7), no matter the element size or the polynomial order used in the discretization [3–5].

To fix this problem we employ a similar approach to that followed in [6, 7] for quasi-static problems. This approach is a simplification of the weighted regularized Maxwell equation method [8] and it consists in removing the divergence term of (7) (the first term on the second line) from the elements which are near the points of the domain where the electric field is singular.

In (2) it is shown that accurate solutions can be obtained with (7) and tetrahedral second order nodal elements if we cancel the divergence term in three layers of elements around any singularity. That is, we must cancel the divergence term in the elements with a node resting on reentrant corners and edges of PECs, corners and edges of dielectrics and on the intersection of several dielectrics [9]. We also have to cancel the divergence term in the elements which are in contact with the previous elements and in the elements which are in contact with these (3 layers). It is possible to use higher order elements and 1 layer, but the computational cost is higher. On the other hand, it was not possible to attain a robust and accurate combination with first-order elements.

Due to the fact that nodal elements impose continuity in all the components of the electric field, we have to consider explicitly the field discontinuities at the interface between different media. At the surfaces separating two different materials we use the double-node strategy explained in [10]. For the intersection of three or more different materials we follow the procedure explained in [2].

The above FEM formulation has been implemented in a C++ in-house code called ERMES (*E*lectric *R*egularized *M*axwell *E*quations with *S*ingularities). ERMES [11] has a user-friendly interface based on the commercial software GiD [12]. GiD is employed for geometrical modeling, meshing and visualization of results. ERMES uses a quasi-minimal residual (QMR) iterative solver [13] with a diagonal preconditioner to solve the linear systems resulting from the finite element discretization. This solver needs one second to finish an iteration of a 2000000 unknowns FEM linear system (as the average ones appearing on this paper) in a desktop computer with a CPU Intel Core 2 Quad Q9300 at 2.5 GHz, 8 GB of RAM memory and

the operative system Microsoft Windows XP Professional x64 Edition v2003.

4. SIMULATIONS

In the next sections we are going to apply the FEM formulation detailed above to three different SAR problems. The essential difference between them is the quantity of singular nodes in the domain. In Section 5, we solve a problem without field singularities. In Section 6, we calculate the SAR produced by an antenna which presents several singular field points. Finally, in Section 7, we solve a problem similar to that in Section 6 but with a higher amount of singular nodes. The objective is to assess the performance of the proposed formulation in real-life SAR problems and show the effect of the singularities in the conditioning of the FEM matrix. To do that we observed the number of iterations required by an iterative solver (QMR with diagonal preconditioning) to reach convergence. In Section 8 we summarize and discuss the results.

5. ELLIPSOIDAL PHANTOM IN RECTANGULAR WAVEGUIDE

In this validation example we compute the SAR in an ellipsoidal phantom placed inside a rectangular waveguide. This experimental set-up is typically found when studying the effect of radiation on small animals [24, 26]. The SAR values obtained with ERMES are compared with measurements and numerical simulations performed with the finite difference time domain method (FDTD).

5.1. Description of the Problem

An ellipsoidal phantom, with a longer axis of 4.1 cm and a shorter axis of 3.0 cm, is filled with a substance of electrical properties $\epsilon = 43\epsilon_0$ and $\sigma = 0.97\,\mathrm{S/m}$. The phantom is placed at the center of a rectangular waveguide WR-975 ($24.76\,\mathrm{cm} \times 12.38\,\mathrm{cm}$) and it is illuminated with the fundamental mode TE_{10}. The incident electric field has a frequency of $f = 900\,\mathrm{MHz}$, a maximum value of $|\mathbf{E}_{\mathrm{rms}}| = \left|\mathbf{E}/\sqrt{2}\right| = 61.4\,\mathrm{V/m}$ and a polarization parallel to the shorter axis of the ellipsoid. The weight of the phantom is $M = 20\,\mathrm{g}$. The weight and electrical properties of the phantom are comparable to those of a mouse. An outline of the problem is shown in Fig. 1. The data for this example are taken from [14].

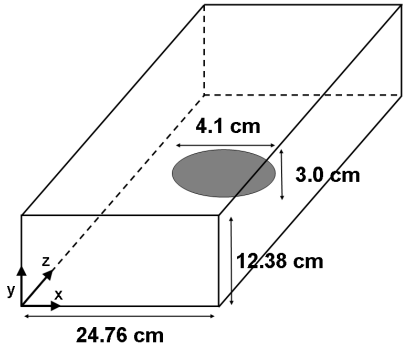

Figure 1. Ellipsoidal phantom inside rectangular waveguide. Data from [14].

5.2. Finite Element Model

We computed the electric field inside the rectangular waveguide with the finite element formulation explained in Section 3. In this example we do not have any field singularity in the problem domain, therefore, we do not need to cancel the divergence term of (7) anywhere. In the metallic walls of the waveguide were used the PEC boundary condition (4). In the waveguide ports we assumed that only the fundamental mode TE_{10} was propagating then, we applied the boundary conditions

$$\begin{aligned} &\hat{\mathbf{n}} \times \nabla \times \mathbf{E} = \gamma \left(\hat{\mathbf{n}} \times \hat{\mathbf{n}} \times \mathbf{E} \right) + \mathbf{U}, \\ &\hat{\mathbf{n}} \cdot \mathbf{E} = 0, \end{aligned} \tag{8}$$

where γ is the propagation constant of the mode TE_{10}, which is $\gamma = \pm i\sqrt{k_0^2 - k_c^2}$ when $k_0 > k_c$ and $\gamma = \mp\sqrt{k_c^2 - k_0^2}$ when $k_0 < k_c$, being $k_0 = \omega\sqrt{\epsilon_0 \mu_0}$ and $k_c = \pi/a$, with a being the width of the rectangular waveguide. The sign of γ depends on the direction of propagation. For the input and the output port, respectively, we have that [15]

$$\begin{aligned} &\mathbf{U} = -2\,\gamma \left(\hat{\mathbf{n}} \times \hat{\mathbf{n}} \times \mathbf{E}_{10} \right), \\ &\mathbf{U} = 0, \end{aligned} \tag{9}$$

where the field $\mathbf{E}_{10}$ is the incident mode TE_{10} imposed in the input port

$$\mathbf{E}_{10} = -\sqrt{\frac{2i\omega\mu}{ab\gamma}}\, \sin(k_c x)\, e^{\gamma z}\, \hat{\mathbf{y}}, \tag{10}$$

being γ the propagation constant, a the width of the rectangular waveguide and b is its height. In (10) we have considered that

the x-axis is along the width of the rectangular waveguide, the y-axis is along its height and the z-axis is perpendicular to the xy-plane. The incident field (10) must be multiplied by the constant $\alpha = 61.4\sqrt{\gamma ab/i\omega\mu} = 0.4776$ to accomplish with the requirement that the maximum value of $|\mathbf{E}_{10}|$ must be $61.4\sqrt{2}$ V/m [14].

Once the electric field is calculated, we obtain the SAR with Equation (1). The density $\rho = M/V$ is deduced using the formula $V = \pi AB^2/6$ for the volume of the ellipsoid, where A is the length of the mayor axis and B the length of the minor axis.

5.3. Results

To solve the above problem were used 347556 tetrahedral second order nodal elements (518735 nodes) which produced a complex linear system with 1311631 unknowns. Our iterative solver reached a residual $r = (\|Ax - b\| / \|b\|) < 1e - 4$ after 1225 iterations (0.09% of the total number of unknowns).

Table 2. SAR averaged over the whole volume of the ellipsoidal phantom. Measurement and FDTD result from [14].

	SAR_{avg} (W/Kg)
Measured	0.06
FDTD	0.05
ERMES	0.05

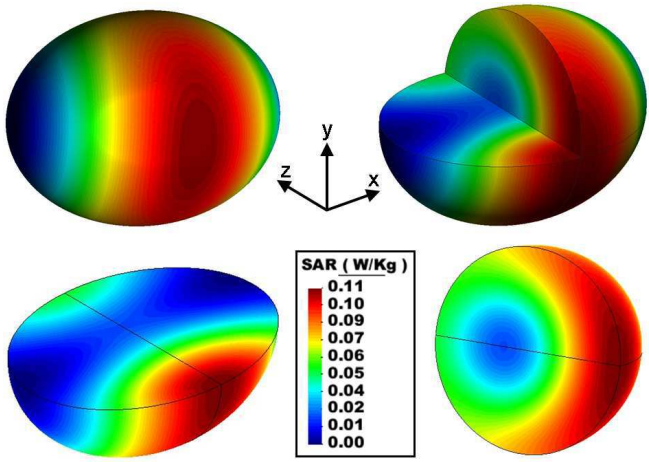

Figure 2. SAR(W/Kg) inside the ellipsoidal phantom.

In Table 2 is showed the SAR averaged over the whole volume of the ellipsoidal phantom (SAR_{avg}). This average SAR can be easily obtained experimentally by measuring the input and the output power in the waveguide ports [14]. On the other hand, the SAR distribution inside the phantom is more difficult to measure and this is where numerical simulations can be very helpful. Fig. 2 shows the SAR distribution inside the phantom. The presence of "hot spots" where the SAR values are several times bigger than the average can be clearly observed with the help of the numerical simulation.

6. PMR ANTENNA NEAR SAM HEAD

In this validation example we compute the SAR produced by a professional mobile radio (PMR) antenna in a specific anthropomorphic mannequin (SAM) head. The results obtained with ERMES are compared with those provided by a commercial software which implements the method of moments (MoM).

6.1. Description of the Problem

A PMR antenna and handset is placed near a SAM head as shown in Fig. 3. The PMR antenna was fed with $P_0 = 2\,\mathrm{W}$ (33 dBm) at a frequency of $f = 390\,\mathrm{MHz}$. The mass density of the SAM head is $\rho = 1000\,\mathrm{Kg/m^3}$ and its electrical properties are $\epsilon = 45.5\epsilon_0$ and $\sigma = 0.7\,\mathrm{S/m}$.

6.2. Finite Element Model

We solved (7) with the PEC boundary condition (4) assigned to the metallic surfaces and the first order absorbing boundary condition (15) assigned to a 70 cm diameter spherical surface centered at the base of the PMR antenna. Also, we used 3 layers of divergence-less elements in the points of the geometry where the field singularities are present (edges of the handset, tip of the PMR antenna and edges of the coaxial feeding).

The PMR antenna was fed by a coaxial waveguide located at its base. We assumed that only the fundamental mode TEM is present in the waveguide port then, we imposed there the following boundary condition

$$\begin{aligned} &\hat{\mathbf{n}} \times \nabla \times \mathbf{E} = \gamma \left(\hat{\mathbf{n}} \times \hat{\mathbf{n}} \times \mathbf{E} \right) + \mathbf{U}, \\ &\hat{\mathbf{n}} \cdot \mathbf{E} = 0 \end{aligned} \tag{11}$$

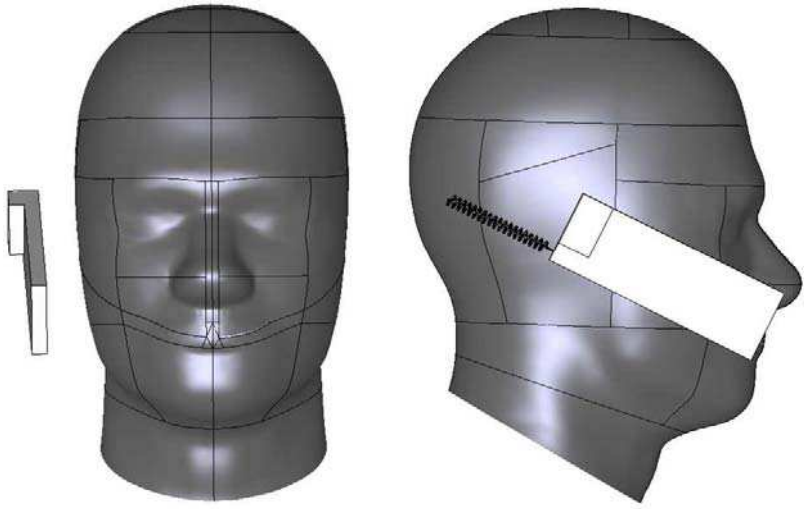

(a) (b)

Figure 3. Positioning of the PMR antenna and handset. (a): Frontal view. (b): Lateral view.

where $\gamma = i\omega\sqrt{\epsilon_0\mu_0}$ is the propagation constant of the fundamental mode and

$$\mathbf{U} = -2\,\gamma\,(\hat{\mathbf{n}} \times \hat{\mathbf{n}} \times \mathbf{E}_{\mathrm{TEM}})\,. \tag{12}$$

The field $\mathbf{E}_{\mathrm{TEM}}$ is the incident field imposed in the input port:

$$\mathbf{E}_{\mathrm{TEM}} = \sqrt{\frac{\eta}{2\pi\ln(b/a)}}\left(\frac{e^{\gamma z}}{\mathrm{r}}\right)\hat{\mathbf{r}}, \tag{13}$$

being $\eta = \sqrt{\mu_0/\epsilon_0}$, $a = 0.60\,\mathrm{mm}$ the inner radius of the coaxial, $b = 1.38\,\mathrm{mm}$ the exterior radius of the coaxial, z is along the direction of propagation, r the radial coordinate and $\hat{\mathbf{r}}$ its unitary vector.

We forced a radiated output power of $P_0 = 2\,\mathrm{W}$ by multiplying the computed $\mathbf{E}$ field by the constant

$$\alpha = \sqrt{\frac{2P_0}{1 - |S_{11}|^2}}, \tag{14}$$

where S_{11} is the reflection coefficient at the coaxial port.

6.3. Results

The problem domain was discretized with 527732 tetrahedral second order nodal elements (791786 nodes). The complex linear system

resulting form the discretization had 1992795 unknowns. The iterative solver reached a residual $r < 1e-4$ after 7965 iterations (0.40% of the total number of unknowns). The results of the simulations performed with ERMES are shown in Figs. 5 and 6. The same problem was

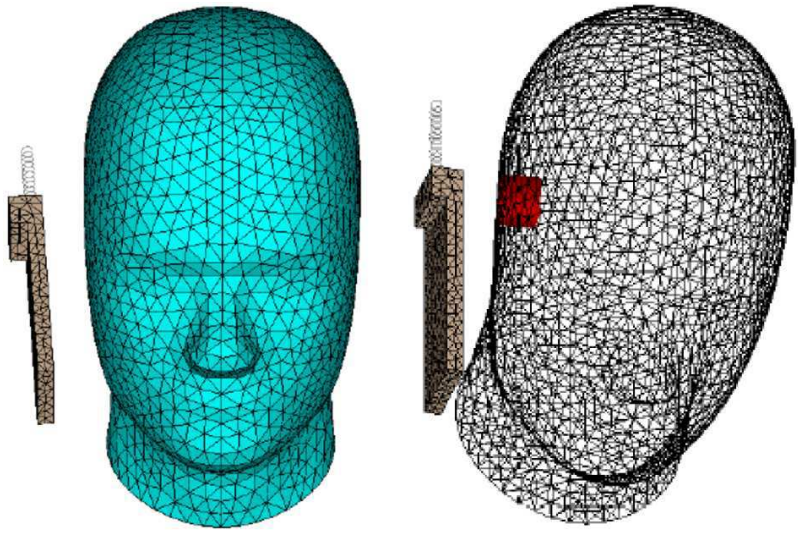

Figure 4. Location of the 10 g cube by FEKO. The SAR averaged over the 10 g cube is 3.20 W/Kg.

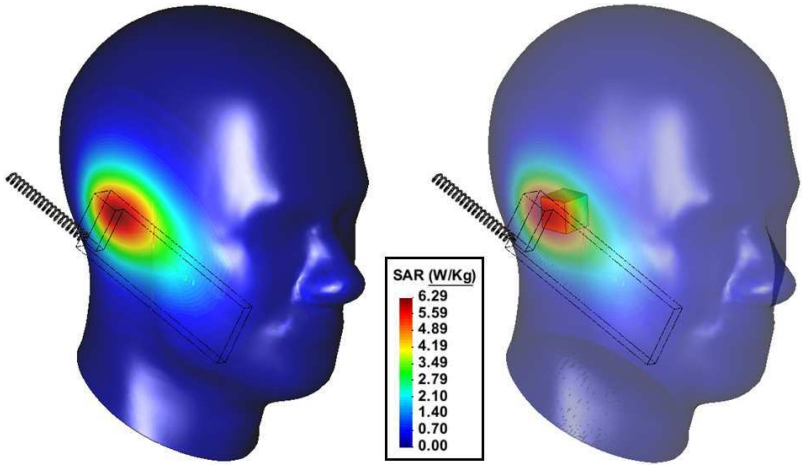

Figure 5. SAR distribution calculated by ERMES and location of the 10 g cube. The maximum SAR is 6.29 W/Kg. The SAR averaged over the 10 g cube is 3.23 W/Kg.

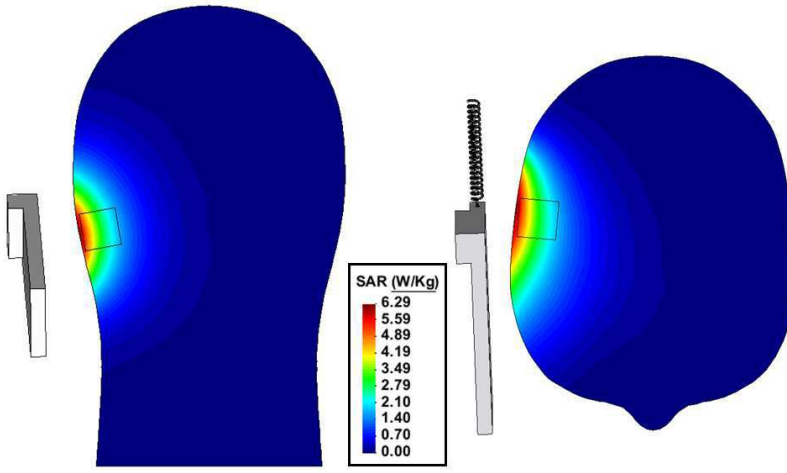

Figure 6. SAR distribution calculated by ERMES. Sections of the SAM head. (a): Frontal view. (b): Upper view.

Table 3. PMR SAR simulations results.

	SAR_{10g} (W/Kg)
FEKO	3.20
ERMES	3.23

solved with FEKO and the results are shown in Fig. 4. In Table 3 are displayed the SAR averaged over the 10 g cube obtained with FEKO and ERMES.

7. PMR-GPS ANTENNA NEAR SAM HEAD

This validation example is similar to that showed in the previous section. We also compute with ERMES the SAR produced by a PMR antenna in a SAM head and compare the results with those provided by FEKO. The main difference is that the total length of the singular edges is larger than in the previous case.

7.1. Description of the Problem

A PMR-GPS antenna prototype designed by Radiall [16] is placed near a SAM head as shown in Fig. 7. At the base of the PMR antenna there

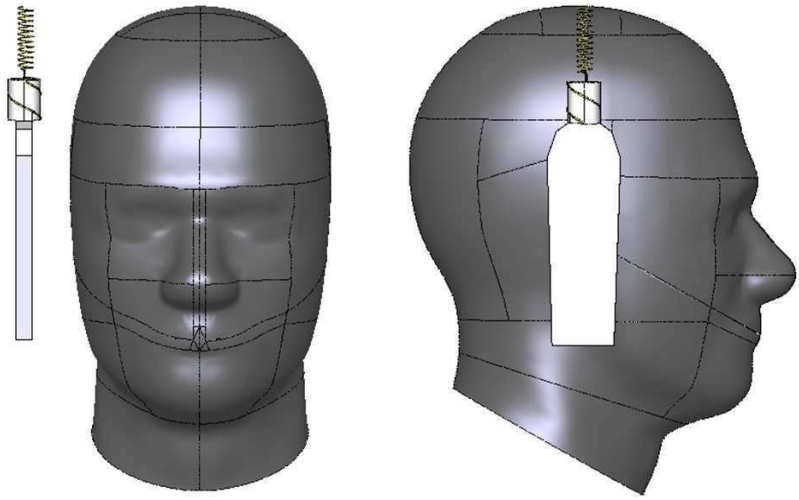

(a) (b)

Figure 7. Positioning of the PMR-GPS antenna. (a): Frontal view. (b): Lateral view. The distance between handset and SAM head is 2 cm.

is a GPS antenna on a cylindrical dielectric substrate with electrical permittivity $\epsilon = 3\epsilon_0$. The PMR antenna was fed with $P_0 = 2\,\mathrm{W}$ (33 dBm) at a frequency of $f = 400\,\mathrm{MHz}$. The SAM head is the same as the one used in Section 6 ($\rho = 1000\,\mathrm{Kg/m}^3$, $\epsilon = 45.5\epsilon_0$ and $\sigma = 0.7\,\mathrm{S/m}$).

7.2. Finite Element Model

We solved (7) with the PEC boundary condition (4) assigned to the surfaces of the PMR antenna, GPS antenna and handset. We also applied the first order absorbing boundary condition

$$\begin{aligned} \hat{\mathbf{n}} \times \nabla \times \mathbf{E} &= i\omega\sqrt{\epsilon_0\mu_0}\,(\hat{\mathbf{n}} \times \hat{\mathbf{n}} \times \mathbf{E})\,, \\ \nabla \cdot \mathbf{E} &= i\omega\sqrt{\epsilon_0\mu_0}\,(\hat{\mathbf{n}} \cdot \mathbf{E})\,, \end{aligned} \tag{15}$$

to a 70 cm diameter spherical surface centered at the base of the PMR antenna. In addition, we used 3 layers of divergence-less elements in the points of the geometry where the field singularities are present (edges of the handset, tip of the PMR antenna, edges of the GPS antenna and edges of the dielectric substrate).

The PMR antenna was fed with a current probe located at its base (see Fig. 8). We imposed a radiated output power of $P_0 = 2\,\mathrm{W}$

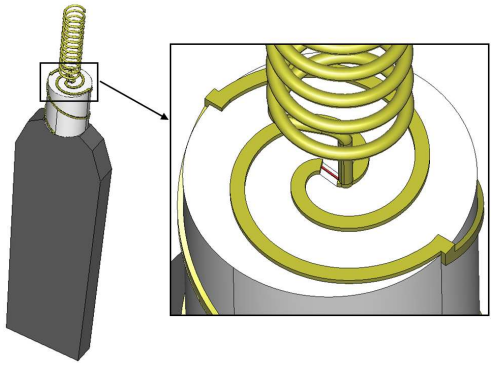

Figure 8. Current probe used by ERMES to fed the PMR-GPS antenna.

by multiplying the computed **E** field by the constant

$$\alpha = \sqrt{\frac{2P_0}{-\int_s \text{Real}\left[\mathbf{E}\cdot\bar{\mathbf{J}}\right]}}, \tag{16}$$

where s is the volume of the current probe.

7.3. Results

The volume contained inside the 70 cm diameter spherical surface was discretized with 838840 tetrahedral second order nodal elements (1336948 nodes). The complex linear system resulting form the discretization had 3286368 unknowns. The iterative solver reached a residual $r < 1e-4$ after 58964 iterations (1.79% of the total number of unknowns). The results of the simulations performed with ERMES are shown in Figs. 9 and 10.

The same problem stated above was computed with the commercial software FEKO [17]. In this case, the antenna feeding was modeled with a voltage gap (see Fig. 11). The results of the simulations performed with FEKO are shown in Fig. 12.

The SAR averaged over the 10 g cube obtained with FEKO and ERMES is displayed in Table 4. The differences in the results can be attributed to the different geometries employed in the computations. We must take into account that the SAR is very sensitive to the positioning of the handset with respect to the SAM head. For instance, if we move the handset 0.4 cm closer to the surface of the SAM head then, the value of the SAR averaged over the 10 g cube obtained with ERMES rises to 3.36 W/Kg.

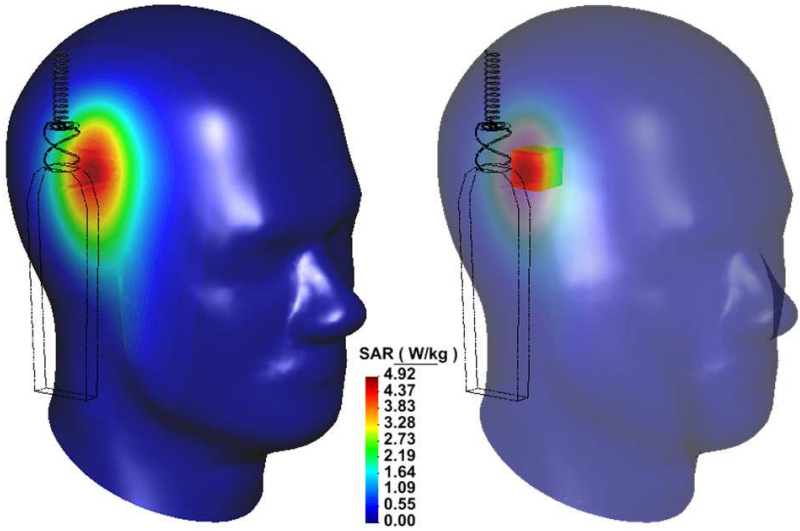

Figure 9. SAR distribution calculated by ERMES and location of the 10 g cube. The maximum SAR is 4.92 W/Kg. The SAR averaged over the 10 g cube is 2.82 W/Kg.

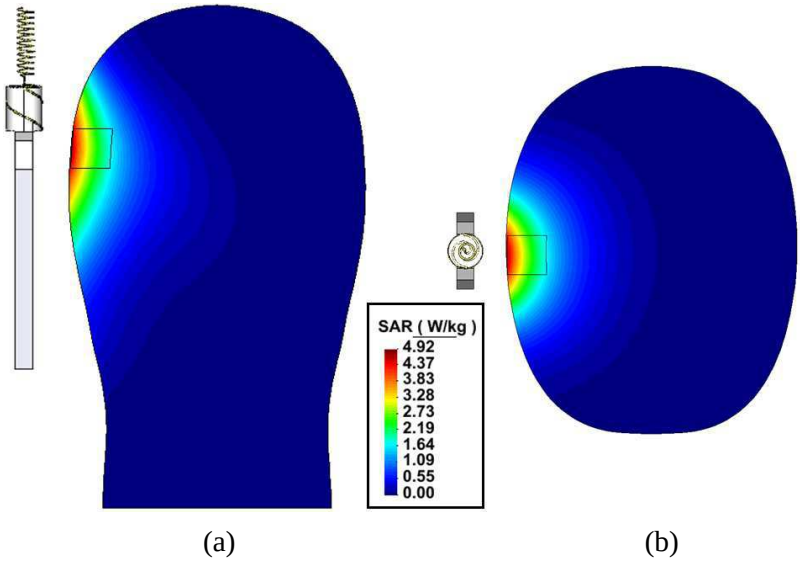

Figure 10. SAR distribution calculated by ERMES. Sections of the SAM head. (a): Frontal view. (b): Upper view.

Table 4. PMR-GPS SAR simulations results.

	SAR_{10g} (W/Kg)
FEKO	3.00
ERMES	2.82

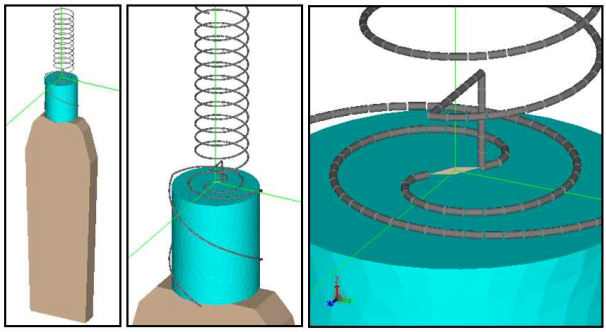

Figure 11. Details of the geometry used by FEKO to model the PMR-GPS antenna. The antenna is fed by a voltage gap.

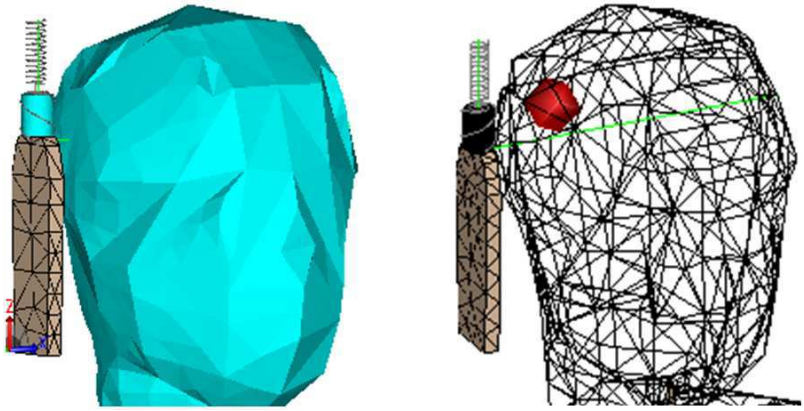

Figure 12. Location of the 10 g cube by FEKO. The SAR averaged over the 10 g cube is 3.00 W/Kg.

8. SUMMARY

In Table 5 are summarized the degrees of freedom and the number of solver iterations of the problems presented in this paper. The effect of the singularities is clearly observed when comparing the solver convergence of the problems showed in Section 5 and reference [18], with the problems showed in Sections 6 and 7 and references [2] and [19]. In the first cases, there are no singularities in the problem

Table 5. Summary table.

	Problem size	Solver iterations
Ellipsoidal phantom	1311631	1225 (0.09%)
PMR antenna	1992795	7965 (0.40%)
PMR-GPS antenna	3286368	58964 (1.79%)

domains and the QMR solver only needs a number of iterations of less than 0.1% of the total number of unknowns to reach convergence. In the second cases, depending of the number of singularities present in the problem domain, this percentage of iterations can be increased up to near 2%.

9. CONCLUSIONS

In this paper we have shown that the computational cost of the proposed nodal-based FEM formulation increases with the number of singular points in the problem domain. This is due to the need of meshing with small elements near the singularity and the worsening of the condition number in the resultant matrix. We can improve the convergence rate using a better solver and preconditioning but, the objective here is to show the effect of the singularities on the FEM matrix. Nevertheless, although the computational cost growth with the increment of singular points, we can still solve efficiently realistic SAR problems in a desktop computer with a very simple iterative solver (QMR with diagonal preconditioning), which proves an acceptable conditioning of the resultant FEM matrix.

It is left for a future work the hybridization of our approach with integral numerical techniques. This hybridization can take profit not only of the low-order singularity kernel of the regularized formulation also of the fact that, usually, in SAR related problems, we can separate dialectic objects (with smooth surfaces) from metallic objects (with sharp edges) and solve the field singularities with the integral numerical method.

ACKNOWLEDGMENT

This work was partially founded by the Spanish Ministry of Industry, Tourism and Commerce in the frame of the project PROFIT SANTTRA (Sistema de Antenas para Transceptores de Radio, Ref: FIT-330210-2006-44) based on the European project PIDEA EUREKA SMART (Smart Antennas System for Radio Transceivers).

REFERENCES

1. Hazard, C. and M. Lenoir, "On the solution of the time-harmonic scattering problems for Maxwells equations," *SIAM Journal on Mathematical Analysis*, Vol. 27, 1597–1630, 1996.
2. Otin, R., "Regularized Maxwell equations and nodal finite elements for electromagnetic field computations," *Electromagnetics*, Vol. 30, 190–204, 2010.
3. Costabel, M. and M. Dauge, "Maxwell and Lamé eigenvalues on polyhedra," *Mathematical Methods in Applied Science*, Vol. 22, 243–258, 1999.
4. Costabel, M., "A coercive bilinear form for Maxwells equations," *Journal of Mathematical Analysis and Applications*, Vol. 157, No. 2, 527–541, 1991.
5. Lohrengel, S. and S. Nicaise, "Singularities and density problems composite materials in electromagnetism," *Communications Differential Equations*, Vol. 27, No. 7, 1575–1623, 2002.
6. Preis, K., O. Bíró, and I. Ticar, "Gauged current vector potential and reetrant corners in the FEM analysis of 3D eddy currents," *IEEE Trans. Magn.*, Vol. 36, 840–843, 2000.
7. Kaltenbacher, M. and S. Reitzinger, "Appropriate finite-element formulation for 3-D electromagnetic-field problems," *IEEE Trans. Magn.*, Vol. 38, 513–516, 2002.
8. Costabel, M. and M. Dauge, "Weighted regularization of Maxwell equations in polyhedral domains," *Numerische Mathematik*, Vol. 93, No. 2, 239–277, 2002.
9. Bladel, J. V., *Singular Electromagnetic Fields and Sources*, IEEE Press, 1991.
10. Paulsen, K. D., D. R. Lynch, and J. W. Strohbehn, "Three-dimensional finite, boundary, and hybrid element solutions of the Maxwell equations for lossy dielectric media," *IEEE Trans. Microw. Theory Tech.*, Vol. 36, 682–693, 1988.
11. Otin, R., "ERMES user guide," International Center for Numerical Methods in Engineering (CIMNE), ref.: IT-617, Tech. Rep., 2011.
12. GiD, the personal pre and post processor, International Center for Numerical Methods in Engineering (CIMNE), Barcelona, Spain, 2010, Available: http://www.gidhome.com.
13. Freund, R. W. and N. M. Nachtigal, "QMR: A quasi-minimal residual method for non-Hermitian linear systems," *SIAM Journal: Numerische Mathematik*, Vol. 60, 315–339, 1991.

14. Kubacki, R., J. Sobiech, J.Kieliszek, and A. Krawczyk, "Comparison of numerical and measurement methods of SAR of ellipsoidal phantoms with muscle tissue electrical parameters," *COMPEL: The International Journal for Computation and Mathematics in Electrical and Electronic Engineering*, Vol. 25, No. 3, 691–696, 2006.
15. Jin, J., *The Finite Element Method in Electromagnetics*, 2nd edition, John Wiley & Sons, 2002.
16. Radiall, "Design, development and manufacturing of connectors, antennas and microwave components," Voreppe, France, 2010, Available: http://www.radiall.com.
17. FEKO, "EM simulation software," 2010, http://www.feko.info.
18. Otin, R., "Numerical study of the thermal effects induced by a RFID antenna in vials of blood plasma," *Progress In Electromagnetics Research Letters*, Vol. 22, 129–138, 2011.
19. Gomez-Calero, C., N. Jamaly, L. Gonzalez, and R. Martinez, "Effect of mutual coupling and human body on MIMO performances," *The 3rd European Conference on Antennas and Propagation (EuCAP)*, 1042–1046, 2009.
20. Bui, V. P., X. C. Wei, and E. P. Li, "An efficient simulation technology for characterizing the ultra-wide band signal propagation in a wireless body area network," *Journal of Electromagnetic Waves and Applications*, Vol. 24, No. 17–18, 2575–2588, 2010.
21. Gao, S., S.-Q. Xiao, H. Zhu, W. Shao, and B.-Z. Wang, "2.45 GHz body-worn planar monopole antenna and its application in body-worn MIMO system," *Journal of Electromagnetic Waves and Applications*, Vol. 25, No. 5–6, 661–671, 2011.
22. Cvetkovi, M., D. Poljak, and A. Peratta, "FETD computation of the temperature distribution induced into a human eye by a pulsed laser," *Progress In Electromagnetics Research*, Vol. 120, 403–421, 2011.
23. Attardo, E. A., T. Isernia, and G. Vecchi, "Field synthesis in inhomogeneous media: Joint control of polarization, uniformity and SAR in MRI B_1-field," *Progress In Electromagnetics Research*, Vol. 118, 355–377, 2011.
24. Angulo, L. D., S. G. Garcia, M. F. Pantoja, C. C. Sanchez, and R. G. Martin, "Improving the SAR distribution in Petri-dish cell cultures," *Journal of Electromagnetic Waves and Applications*, Vol. 24, No. 5–6, 815–826, 2010.
25. Mohsin, S. A., "Concentration of the specific absorption rate

around deep brain stimulation electrodes during MRI," *Progress In Electromagnetics Research*, Vol. 121, 469–484, 2011.

26. Jorge-Mora, T., M. Alvarez-Folgueiras, J. M. Leiro, F. J. Jorge-Barreiro, F. J. Ares-Pena, and E. Lopez-Martin, "Exposure to 2.45 GHz microwave radiation provokes cerebral changes in induction of HSP-90 α/β heat shock protein in rat," *Progress In Electromagnetics Research*, Vol. 100, 351–379, 2010.
27. Parise, M., "On the use of cloverleaf coils to induce therapeutic heating in tissues," *Journal of Electromagnetic Waves and Applications*, Vol. 25, No. 11–12, 1667–1677, 2011.
28. Zhang, M. and A. Alden, "Calculation of whole-body SAR from a 100 MHz dipole antenna," *Progress In Electromagnetics Research*, Vol. 119, 133–153, 2011.